Electronic Structure and Low-Lying Electronic States of Al_3O and Al_3O^-: Photoelectron Spectrum of Al_3O^-

Tapan K. Ghanty[†] and Ernest R. Davidson*

Department of Chemistry, Indiana University, Bloomington, Indiana 47405

Received: November 30, 1998; In Final Form: February 8, 1999

We have calculated the equilibrium geometries of the ground electronic state of Al_3O and Al_3O^- using Hartree−Fock, density functional, and coupled-cluster doubles methods. These molecules are nominally equilateral triangles of Al atoms with an oxygen in the center which distort due to the Jahn−Teller effect. The calculated global minima had C_{2v} symmetry with $(b_2)^1\ ^2B_2$ and $(b_2)^2\ ^1A_1$ configurations, respectively. The global minimum of the lowest triplet state of Al_3O^- was found to have D_{3h} symmetry with an $(e')^2\ ^3A_2'$ electron configuration. While this was the lowest energy state of the molecule among D_{3h} symmetry points, this triplet minimum had slightly higher energy than the $^1A_1$ state at its C_{2v} global minimum. The $^1A_1\ (a_1)^2$ and the $^1B_2\ (b_2)^1(a_1)^1$ configurations of Al_3O^- and the $^2A_1\ (a_1)^1$ configuration of Al_3O lead to transition states of C_{2v} symmetry on the respective potential energy surfaces for pseudorotation. Using the CCD geometries of $(b_2)^2\ ^1A_1$ and $(e')^2\ ^3A_2'$ Al_3O^-, configuration interaction calculations have been performed to determine the low-lying vertical excited states of Al_3O, and those results have been utilized to interpret the recently reported experimental photoelectron spectrum of Al_3O^-. On the basis of the present CI results, new assignments have been made for some of the peaks.

Introduction

Electron correlation plays an important role for a detailed understanding of the electronic structure of atoms and molecules. The correlation energy, defined as the difference between the nonrelativistic exact energy and the Hartree−Fock energy, is very small compared to the Hartree−Fock energy. The change in correlation energy in a chemical process is usually of the same order of magnitude as the energy differences of chemical interest. Apart from the effect on energy, electron correlation effects are also manifested in the intensity of the photoelectron spectrum of atoms and molecules.

One direct experimental method for obtaining electron binding energy for each orbital is photoelectron spectroscopy (PES). The interpretation of photoelectron spectra has benefited tremendously from simple molecular orbital (MO) models like Hartree−Fock theory, which has been successful in accounting for the main features of photoelectron spectra, especially in the outer valence region. Generally, there is a one-to-one correspondence between the valence molecular orbitals and main ionization peaks. However, simple MO theory cannot account for the lower intensity "extra" peaks that are very often observed.[1] These extra peaks are called "correlation peaks" (although they are also referred to as satellite peaks, shake-up peaks, or many-body peaks), and have zero intensity in the Hartree−Fock model. It is precisely from the effect of electron correlation in atomic or molecular systems that these peaks gain intensity and appear in the photoelectron spectra. Recent benchmark configuration interaction (CI) calculations[2−6] have been able to interpret and predict the electron binding energy spectra of a number of molecular systems. Besides CI, Green's function methods have also been used extensively[7] to explain the observed photoelectron spectra of molecules.

In recent years, metal clusters have been the subject of several experimental and theoretical investigations[8,9] to understand the electronic structure and bonding, not only for the ground electronic state but also for the low-lying excited electronic states. Due to the likely presence of a large number of closely spaced excited states, it is rather a challenging job to provide a list of the excited states in correct energy order. "Hypermetallic molecules" involving metal stoichiometries exceeding normal valence expectations are now well documented experimentally[9] and have been extensively studied theoretically.[10−12] These species can be regarded as metal clusters bound ionically to a centrally located nonmetallic atom.

Within this class of molecules, Al_3O has been studied both experimentally[10−12] and theoretically.[13−17] Very recently, the photoelectron spectrum of Al_3O^- has also been reported[18] at several photon energies. Although the ground state of neutral Al_3O has been studied theoretically before,[13] to our knowledge there is no theoretical report on the ground state of Al_3O^- or on excited states of Al_3O. In order to understand the features in the experimental photoelectron spectrum of Al_3O^-, one should have reliable theoretical results for many electronic states of Al_3O and also for all thermally accessible states of Al_3O^-. The purpose of this work is to calculate the ground-state geometry of Al_3O^-, and the electronic structures and the energies of the low-lying excited states of Al_3O in order to interpret the experimentally observed photoelectron spectrum. Because of complications caused by Jahn−Teller effects (see Results section) computational methods appropriate for degenerate biradicals must be used.

Theoretical Methods

The geometries of neutral and anionic Al_3O were optimized employing ROHF (restricted open shell Hartree−Fock), TCSCF

* Corresponding author.
[†] On leave from the Chemistry Division, Bhabha Atomic Research Centre, Trombay, Bombay 400 085, India.

10.1021/jp984555g CCC: $18.00
Published on Web 03/20/1999

TABLE 1: Calculated Bond Lengths and Bond Angles of Low-Lying Electronic States of Al_3O and Al_3O^- by Different Methods[a]

method	state	R_1	$R_2 = R_3$	θ_1	energy (E_h)	ΔE (kcal/mol)
			Al_3O			
ROHF/6-31+G*	$^2B_2$	2.001	1.800	151.6	−800.638 796	0.
ROHF/6-31+G*	$^2A_1$	1.764	1.918	96.0	−800.639 073	−0.17
UB3LYP/6-31+G*	$^2B_2$	1.992	1.835	163.0	−802.591 550	0.
UB3LYP/6-31+G*	$^2A_1$	1.780	1.950	91.9	−802.587 225	2.71
UCCD/6-31+G*	$^2B_2$	1.985	1.829	156.8	−800.996 762	0.
UCCD/6-31+G*	$^2A_1$	1.780	1.939	91.8	−800.996 542	0.14
UCCSD(T)/6-31+G*	$^2B_2$				−801.018 057	0.
UCCSD(T)/6-31+G*	$^2A_1$				−801.016 464	1.00
			Al_3O^-			
TCSCF/6-31+G*	$^1A_1(b_2^2)$	1.959	1.811	170.8	−800.652 661	0.
TCSCF/6-31+G*	$^1A_1(a_1^2)$	1.720	1.948	92.2	−800.642 288	6.51
ROHF/6-31+G*	$^3A_2'(e'^2)$	1.844	1.844	120.0	−800.649 131	2.21
ROHF/6-31+G*	$^1B_2(a_1b_2)$	1.909	1.833	104.1	−800.638 022	9.19
B3LYP/6-31+G*	$^1A_1(b_2^2)$	2.012	1.835	177.1	−802.629 547	0.
B3LYP/6-31+G*	$^1A_1(a_1^2)$	1.735	1.987	87.1	−802.606 521	14.45
UB3LYP/6-31+G*	$^3A_2'(e'^2)$	1.866	1.866	120.0	−802.612 797	10.51
CCD/6-31+G*	$^1A_1(b_2^2)$	1.999	1.828	177.5	−801.023 210	0.
CCD/6-31+G*	$^1A_1(a_1^2)$	1.735	1.970	87.2	−801.006 308	10.61
UCCD/6-31+G*	$^3A_2'(e'^2)$	1.860	1.860	120.0	−801.012 581	6.67
CCSD(T)/6-31+G*	$^1A_1(b_2^2)$				−801.047 152	0.00
CCSD(T)/6-31+G*	$^1A_1(a_1^2)$				−801.027 830	12.12
UCCSD(T)/6-31+G*	$^3A_2'(e'^2)$				−801.031 559	9.78

[a] For each method energy difference calculated with relative to the $^2B_2$ and $^1A_1(b^2)$ state energies of Al_3O and Al_3O^-, respectively. CCSD(T) energies are calculated at the corresponding CCD optimized geometries. All structures have C_{2v} symmetry with the oxygen near the center of a triangle formed by the aluminum atoms. R_1 is the unique Al1O distance while R_2 and R_3 are the Al2O and Al3O distances. θ is the unique Al2OAl3 angle while Al1OAl3 and Al2OAl3 define θ_2 and θ_3 which are each $180° - \theta/2$.

(two-configuration self-consistent field), density functional theory (DFT) with B3LYP (three-parameter Becke exchange and Lee−Yang−Parr correlation), and the coupled-cluster doubles (CCD) methods with the 6-31+G* basis set. For DFT and CCD calculations, the Gaussian 94[19] program was used, whereas for ROHF and TCSCF calculations, the HONDO[20] program was used. Utilizing these optimized geometries, CI calculations were performed using the MELD[21] program. The basis set used for the CI calculation is aug-cc-pVTZ excluding the *f* function and augmenting *d* function.[22] This basis set is motivated by the need to represent all Al_3O states up to an excitation energy of about 10 eV with CI calculations that are still computationally affordable. The starting orbitals for CI wave functions were obtained from ground state Al_3O^- ROHF computations. The canonical virtual orbitals are converted to K orbitals[23] to carry out the CI calculations. The 1*s*, 2*s*, and 2*p* electrons of aluminum and 1*s* electrons of oxygen were kept frozen as the core and the remaining valence electrons were treated explicitly in the CI calculations.

Within a closed-shell Hartree−Fock approximation, an *N*-electron molecule can be represented as $\Psi_{HF}(N)$ (the ground state wave function). A primary hole configuration $\Psi_k(N-1)$ (which corresponds to removal of an electron from the *k*th occupied orbital) can be written as $\Psi_k(N-1) = a_k\Psi_{HF}(N)$, where a_k is an annihilation operator that destroys orbital *k* in $\Psi_{HF}(N)$. According to Koopmans' theorem, the position of the peaks corresponding to the *n* occupied orbitals will be given by the negative of their orbital energies. However, as mentioned before, the independent particle model is not adequate to explain the appearance of correlation peaks in photoelectron spectra. There can be excitations followed by ionization, like $1p-2h$ (one particle−two holes), $2p-3h$ (two particles-three holes), etc. Therefore, the wave functions for the ground state of the neutral, $\Psi(N)$, or any state of the ion, $\Psi_k(N-1)$, are written as linear combinations of all possible configurations in the CI method.

The pole strength or intensity of the transition for the *k*th ionic state is defined as

$$S_k^2 = ||\langle\Psi_k(N-1)|\Psi(N)\rangle_{N-1}||^2$$

where the integration is performed over $N-1$ electrons. The pole strength of the peak corresponding to the $0p-1h$ (primary peak) ionic state configuration will be close to unity and the pole strengths of the peaks associated with other configurations ($1p-2h$, $2p-3h$, etc.) are usually very small ($S_k^2 \ll 1$). The photoelectron peak intensities are proportional to the pole strength multiplied by the squares of transition moments between the bound orbital and the continuum.

For open-shell initial and final states, the intensities must be averaged over degenerate initial states and summed over degenerate final states; i.e., the weight *w* of the transition in the system is given by

$$w = \sum_{\text{initial}}\sum_{\text{final}} S_{\text{if}}^2/g$$

where *g* is the degeneracy of the initial state. For the simplest possible open-shell wave functions formed by symmetry-determined linear combinations of Slater determinants using spin and symmetry-constrained orbitals, the sum of *w* would still be the number of active electrons when summed over all roots of the CI matrix.

Results

The calculated ground state geometrical parameters and energies for Al_3O and Al_3O^- are reported in Table 1. Figure 1 shows the orbital energies and labels for Al_3O^-. Bonding in these molecules is quite unusual. They are most simply considered to have three Al^+ ions arranged in an equilateral triangle and attached to a central O^{2-} by coordinate covalent bonds between oxygen sp^2 lone pairs and empty Al $p\sigma$ orbitals.

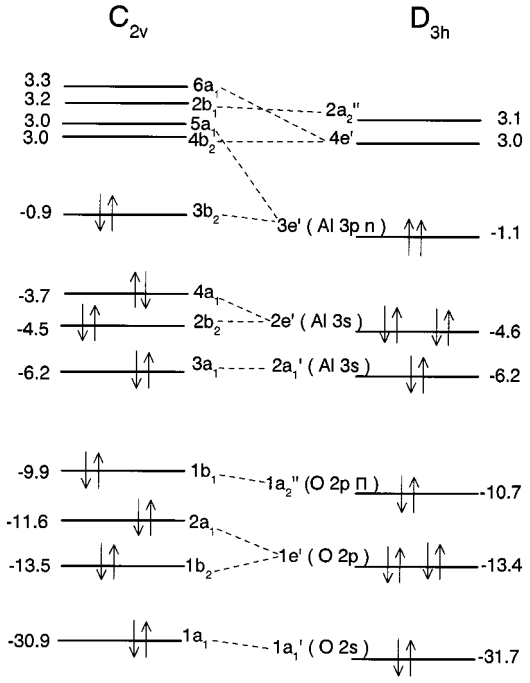

Figure 1. Orbital energy (eV) diagram for Al_3O^- $3b_2^2\ {}^1A_1$ and $3e'^2\ {}^3A'^2$ states.

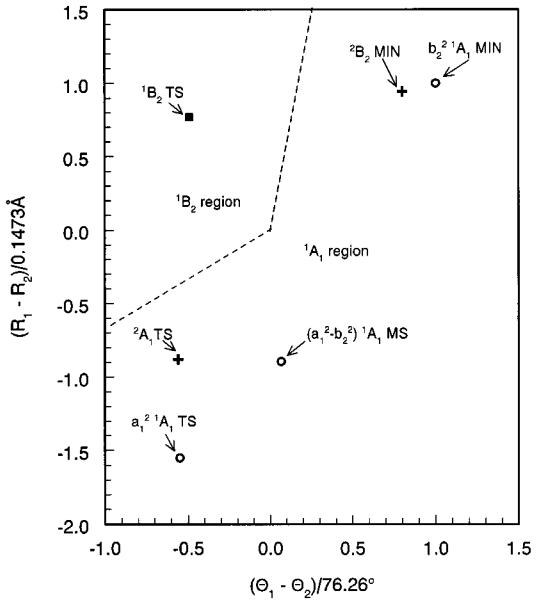

Figure 2. Plot indicating the regions of different electronic wave function symmetry on the ground state potential energy surface of Al_3O^-. Location of minima (MIN) and transition states (TS) are indicated along with the monkey saddle (MS). The stationary points for neutral Al_3O are also indicated by +. The TSs are each a relative minimum in this plane with an imaginary frequency for a b_2 normal mode.

The Al is essentially unhybridized. The remaining two electrons of Al_3O^- (or remaining one electron of Al_3O) are placed in an e' (in D_{3h} symmetry) linear combination of *pn* Al atomic orbitals (*p* orbitals in the plane but orthogonal to the Al−O bond). The remaining $p\pi$ electron pair of O^{2-} participates to some extent also in coordinate covalent bonding with the empty $p\pi$ orbitals of Al and is the only occupied out-of-plane molecular orbital.

This model predicts that Al_3O should have a $e'\ {}^2E'$ ground state. This is subject to Jahn−Teller distortion. The simplest result would be distortion to a C_{2v} shape with distortion in one direction leading to a minimum and distortion in the opposite direction leading to a transition state for pseudorotation. That is, one of these points would have all real frequencies and the other would have one imaginary frequency for a normal mode that broke C_{2v} symmetry. Since Al_3O has two e' vibrational modes, one associated with angle bending and one with bond stretching, the picture is a little more complicated. As is easily shown,[24] one linear combination of these normal modes will be Jahn−Teller active and the other combination will be inactive. For the neutral molecule, it turns out that the active mode simultaneously stretches the Al−O bond to the unique atom (in C_{2v} symmetry) and opens the angle opposite that atom. Figure 2 depicts this situation for Al_3O. Along the positive phase of this distortion the ground state wave function is the $^2B_2$ component of the $^2E'$ state, while along the negative phase the lowest state is the $^2A_1$ component. It is not possible, a priori, to say which of these distortions will lead to the minimum and which to the transition state.

From Table 1, one can see that for Al_3O, the $^2A_1$ form with a negative phase of distortion (decrease of the unique bond length and opposite angle) is predicted to be the minimum with ROHF calculations. With better methods like UB3LYP and CCSD(T) (coupled-cluster for single and double excitations and perturbation treatment of triple excitations), the positive phase of distortion with a $^2B_2$ wave function gives the lower energy. The nature of these stationary points was confirmed by frequency calculations. These findings are consistent with earlier results[13] in which UHF/6-31G* gave a negative distortion with a $^2A_1$ global minimum while UMP2/6-31G* calculations gave a positive phase and a $^2B_2$ wave function at the global minimum.

The valence electron configurations (core orbitals are not included in the numbering scheme) for the $^2B_2$ and $^2A_1$ structures have been found to be $...(4a_1)^2(2b_2)^2(3b_2)^1$ and $...(4a_1)^2(2b_2)^2(5a_1)^1$, respectively. It is to be noted that in the paper by Boldyrev and Schleyer,[13] the electron configurations for both the $^2B_2$ and $^2A_1$ states were reported incorrectly as $...(4a_1)^2(2b_1)^2(2b_2)^1$ and $...(4a_1)^2(2b_1)^2(5a_1)^1$. This is just a transcription error, however, as we have verified their numerical results using the correct configuration. On the other hand, Wu et al.[18] based their assignment of the photoelectron spectrum of Al_3O^- on this mistyped configuration for Al_3O.

From Table 1, one can compare the energy difference between the $^2B_2$ and $^2A_1$ states of neutral Al_3O. With the ROHF method and a 6-31+G* basis, the $^2A_1$ state is found to be more stable by 0.2 kcal/mol, whereas with UB3LYP, CCD, and CCSD(T) methods, the $^2B_2$ state is found to be more stable by 2.7, 0.1, and 1.0 kcal/mol, respectively. It is interesting to compare the present results with earlier reported[13] energy differences of 1.4 kcal/mol with $^2A_1$ more stable (UHF/6-31G*), compared to 1.1 kcal/mol (UMP2/6-31G*) and 0.5 kcal/mol (UMP4/6-311+G*) with $^2B_2$ more stable. In the present work, we have not considered the $D_{3h}(^2E)$ structure for the neutral Al_3O as it has been found[13] to be a high energy structure.

For Al_3O^-, so far there has not been any experimental or theoretical report on the geometry or the electronic structure. Following the same reasoning as for Al_3O, we would expect four low-energy wave functions at a D_{3h} geometry with e'^2 configuration. Hund's rule suggests the lowest state should be $^3A_2'$. In the notation of the orbitals after C_{2v} distortion, the next two wave functions would be the $^1(a_1b_2)$ and $(a_1^2 - b_2^2)$ components of a $^1E'$ state. Finally, there would be a higher energy $^1A_1'$ state with configuration $(a_1^2 + b_2^2)$. Notice that none of these singlet states can be properly described by one Slater determinant. All are biradicals and require a multireference

starting point. The minimum description is a two-electron/two-orbital CASSCF (complete active space SCF). For the $^1(a_1b_2)$ wave function this is an open-shell singlet ROHF function, while for the $(a_1^2 - b_2^2)$ function a TCSCF (two configuration SCF) calculation is required. No single reference method such as DFT or CCD is appropriate for these states.

As before, the $^1E'$ state is subject to Jahn−Teller distortion. Using the TCSCF and ROHF methods, we have calculated several points of the lowest energy potential energy surface of Al_3O^- and plotted the results in Figure 2 as (R_1-R_2) vs $(\theta_1-\theta_2)$, where R_1 is the bond length of the unique Al−O bond (in C_{2v} symmetry) and θ_1 is the unique bond angle, and R_2 and θ_2 are the other bond lengths and bond angles, respectively. Figure 2 divides the C_{2v} distortion plane into a region where the lowest singlet state is $^1B_2$ and a region where it is $^1A_1$. In the case of Al_3O^-, the Jahn−Teller active mode is now stretch of the unique bond with simultaneous compression of the opposite angle. The positive phase of this distortion leads to a $^1B_2$ wave function for the lowest energy singlet state while the opposite phase leads to $^1A_1$. Along the dividing line between the $^1A_1$ and $^1B_2$ regions the energy is degenerate. This line is the locus of a branch cut in the potential energy surface.[24] When all six internal coordinates are considered, this branch-out is seen to be four-dimensional.

We have found that the $^1A_1$ configuration gives the global minimum of Al_3O^-. This is found to have C_{2v} symmetry and the TCSCF wave function is mostly $...(4a_1)^2(2b_2)^2(3b_2)^2$ with only a small amount of $...(4a_1)^2(2b_2)^2(5a_1)^2$. As Figure 2 shows, this $^1A_1$ minimum is not simply the opposite phase distortion from the $^1B_2$ transition state. This is an interesting illustration of a so-called pseudo-Jahn−Teller effect. After C_{2v} distortion, the $(a_1^2 - b_2^2)$ and $(a_1^2 + b_2^2)$ D_{3h} wave functions have the same C_{2v} symmetry and can be strongly mixed by C_{2v} distortions. This effect is often invoked to explain the existence of broken symmetry double minima, as in the rectangular distortion of cyclobutadiene.[25] In the case of Al_3O^-, it appears that this mixing is strongest in the combination of bond stretching and angle distortions orthogonal to the one that is Jahn−Teller active. After distortion in this mode, there are two $^1A_1$ stationary points. At one, the wave function is predominantly a_1^2 and at the other it is b_2^2. The b_2^2 stationary point is found to be a true minimum while the a_1^2 stationary point has one imaginary frequency for a normal mode that breaks the C_{2v} symmetry. Based on these TCSCF results, it appears that a single reference SCF or DFT calculation should produce a reasonable result in the neighborhood of the b_2^2 $^1A_1$ minimum. It is interesting to note that the Al_3O^- $^1A_1$ $(b_2)^2$ and $^1A_1$ $(a_1)^2$ stationary point geometries are close to the corresponding neutral Al_3O $^2B_2$ $(b_2)^1$ and $^2A_1$ $(a_1)^1$ stationary point geometries, respectively. These two $^1A_1$ stationary points in Figure 2 are connected by a monkey saddle which has two imaginary frequencies. One of these frequencies is for the b_2 normal mode that destroys C_{2v} symmetry while the other is for an a_1 normal mode connecting the a^2 and b^2 $^1A_1$ stationary points. At the monkey saddle, the wave function is nearly $(a_1^2 - b_2^2)$.

We have also considered the first triplet state of Al_3O^- and have found that it has a global minimum at a D_{3h} geometry with the $...(2e')^4(3e')^2$ $^3A_2'$ configuration. All the calculated vibrational frequencies are real for this triplet minimum. This triplet minimum is slightly higher in energy than the b_2^2 $^1A_1$ minimum energy C_{2v} structure. This is not a violation of Hund's rule since the triplet state is the lowest energy state at its D_{3h} minimum. It can be noticed from Table 1 that for Al_3O^-, the relative energy order at the stationary points is $^1A_1(b_2^2)[C_{2v}] < {}^3A_2'$ $(a_1^1\ b_2^1)[D_{3h}] < {}^1A_1(a_1^2)$ $[C_{2v}] < {}^1B_2$ $(a_1^1\ b_2^1)[C_{2v}]$. With the TCSCF method, the difference in energy between the global minimum singlet and triplet structures (i.e., $^1A_1(b_2^2)[C_{2v}]$ and $^3A_2'$ $(e'^2)[D_{3h}]$) is small (2.2 kcal/mol) compared to UB3LYP (10.5 kcal/mol), UCCD (6.7 kcal/mol), and UCCSD(T) (9.8 kcal/mol) methods.

TABLE 2: Calculated[a] Line Positions and Intensities for the Photoelectron Spectrum of Al_3O^-

state	binding energy[b] (eV)	intensity[c] (S_j^2)	important configurations[d]
$^2B_2$	1.68	0.89	$0.93(3b_2)^{-1}$
$^2A_1$	3.51	0.76	$0.84(4a_1)^{-1}$; $0.30(3b_2)^{-2}$ $(5a_1)^1$
$^2B_2$	3.94	0.79	$0.85(2b_2)^{-1}$; $0.21(3b_2)^{-1}$ $(4a_1)^{-1}$ $(5a_1)^1$
$^2A_1$	4.61	0.15	$0.73(3b_2)^{-2}$ $(5a_1)^1$; $0.27(4a_1)^{-1}$
$^2A_1$	5.22	0.56	$0.71(3a_1)^{-1}$; $0.39(2b_2)^{-1}$ $(3b_2)^{-1}$ $(5a_1)^{-1}$; $0.26(3b_2)^{-2}$ $(5a_1)^1$
$^2A_1$	6.01	0.07	$0.51(3b_2)^{-2}$ $(8a_1)^1$; $0.36(3b_2)^{-2}$ $(na_1)^1$; $0.24(3b_2)^{-2}$ $(7a_1)^1$
$^2B_1$	6.76	0.06	$0.35(4a_1)^{-1}$ $(3b_2)^{-1}$ $(2a_2)^1$; $0.28(2b_2)^{-1}$ $(3b_2)^{-1}$ $(3b_1)^1$ $0.28(2b_2)^{-1}$ $(3b_2)^{-1}$ $(2b_1)^1$; $0.26(3b_2)^{-2}$ $(2b_1)^1$
$^2B_1$	6.81	0.76	$0.86(1b_1)^{-1}$
$^2A_1$	7.73	0.07	$0.43(2b_2)^{-1}$ $(3b_2)^{-1}$ $(5a_1)^1$; $0.28(4a_1)^{-2}$ $(5a_1)^1$; $0.21(3a_1)^{-1}$
$^2A_1$	8.07	0.25	$0.49(2a_1)^{-1}$; $0.41(4a_1)^{-2}$ $(5a_1)^1$; $0.28(2b_2)^{-2}$ $(5a_1)^1$
$^2A_1$	8.18	0.10	$0.37(2b_2)^{-1}$ $(3b_2)^{-1}$ $(5a_1)^1$; $0.35(3b_2)^{-2}$ $(na_1)^1$ $0.30(3b_2)^{-2}$ $(n'a_1)^1$
$^2A_1$	8.65	0.31	$0.50(2a_1)^{-1}$; $0.31(2b_2)^{-2}$ $(5a_1)^1$; $0.30(2b_2)^{-1}$ $(3b_2)^{-1}$ $(5a_1)^1$
$^2B_2$	9.74	0.06	$0.38(3b_2)^{-1}$ $(3a_1)^{-1}$ $(5a_1)^1$; $0.27(2b_2)^{-1}$ $(4a_1)^{-1}$ $(5a_1)^1$ $0.24(1b_2)^{-1}$; $0.23(3a_1)^{-1}$ $(2b_2)^{-1}$ $(5a_1)^1$

[a] For each symmetry, the $2h-1p$ wave functions were used for the anion and neutral molecule. The transitions from $^1A_1$ state of Al_3O^- (C_{2v}) have been considered. [b] The first $^2B_2$ state energy was adjusted to experimental data (1.68 eV) and the same constant shift used for all other states. [c] The values less than 0.05 were not listed. [d] The absolute values for the CI coefficients were taken. All molecular orbitals of higher energy than $8a_1$ were denoted as na_1 or $n'a_1$.

In Table 2 we have reported the results of $2h-1p$ CI calculations for different excited states of Al_3O. Here only the vertical transitions from the $^1A_1$ $(b_2^2)[C_{2v}]$ minimum of Al_3O^- to various states of Al_3O have been considered. The energy of all roots has been shifted by a constant so the lowest energy root ($^2B_2$) agrees with the corresponding 1.68 eV vertical ionization peak in the experimental spectrum. For the negative ion of Al_3O^- ($^1A_1$ state) a small CI calculation was done and, using both the negative ion wave function and neutral wave functions, pole strength values were calculated for different states. In addition to the binding energies, this Table 2 also includes the calculated pole strength values (S_j^2) and the leading terms in the wave function for each state. For each symmetry the lowest 20 roots are considered and only those states whose calculated pole strength value is greater than 0.05 have been listed in the table. From Table 2 it can be seen that the primary hole states associated with ionization from the $3b_2$, $4a_1$, $2b_2$, $3a_1$, and $1b_1$ orbitals can be easily identified. It is harder to identify the primary or parent hole states corresponding to the ionization of the $2a_1$ or $1a_1$ orbitals since the CI coefficients for these configurations are small in all states due to the high correlation effects.

If one considers only the allowed transitions from the $^1A_1$ state of Al_3O^- to different states of neutral Al_3O, all the features in the experimental spectrum cannot be explained. In order to

TABLE 3: Calculated[a] Line Positions and Intensities for the Photoelectron Spectrum of Al_3O^-

state	binding energy[b] (eV)	intensity[c] (S_j^2)	important configurations[d]
$^2E'$	1.22	0.91	$0.94(3e')^{-1}$
$^4E'$	3.30	1.03	$0.87\ (2e')^{-1}$; $0.21(2e')^{-1}(3e')^{-1}(4e')^1$
$^2E'$	3.77	0.12	$0.87(2e')^{-1}$; $0.22(2a_1')^{-1}(3e')^{-1}(4e')^1$
$^2E'$	4.23	0.26	$0.76(2e')^{-1}$; $0.41(2a_1')^{-1}$
$^4A_2'$	4.59	0.90	$0.84(2a_1')^{-1}$; $0.37(2e')^{-1}(3e')^{-1}(4e')$
$^2E'$	5.35	0.19	$0.69(2e')^{-1}$; $0.36(2a_1')^{-1}$; $0.25(2e')^{-1}(3e')^{-1}(4e')^1$
$^2A_2'$	6.70	0.05	$0.723(2e')^{-2}(3e')^1$; $0.40(2a_1')^{-1}(2e')^{-1}(3e')^1$; $0.28\ (2a_1')^{-1}$
$^4A_1''$	6.80	1.10	$0.90(1a2'')^{-1}$
$^2A_1''$	6.90	0.55	$0.90(1a2'')^{-1}$
$^2A_2'$	7.02	0.42	$0.77(2a_1')^{-1}$; $0.20(2a_1')^{-1}(2e')-1(3e')^1$
$^4E'$	8.37	0.17	$0.36(1e')^{-1}$; $0.30(2e')^{-1}(3e')^{-1}(5e')^1$; $0.23(2e')^{-1}(3e')^{-1}(4e')^1$
$^4A_2'$	8.63	0.11	$0.63(2e')^{-1}(3e')^{-1}(4e')^1$; $0.29(2a_1')^{-1}$
$^4E'$	8.67	0.35	$0.53(1e')^{-1}$; $0.32(2a_1')^{-1}(3e')^{-1}(4e')^1$
$^4E'$	9.39	0.18	$0.36(1e')^{-1}$; $0.36(2e')^{-2}(4e')^1$; $0.29(2e')^{-1}(3e')^{-1}(na_1')^1$
$^4A_1'$	9.58	0.05	$0.42(2e')^{-1}(3e')^{-1}(na_1')^1$; $0.24(2a_1')^{-1}(3e')^{-1}(na_1')^1$ $0.28(2e')^{-1}(3e')^{-1}(n'a_1')^1$

[a] For each symmetry, the $2h-1p$ wave functions were used for the anion and neutral molecule. The transitions from the $^3A_2'$ state of Al_3O^- (D_{3h} symmetry) have been considered. [b] The first $^2E'$ state energy was adjusted to experimental data (1.22 eV) and the same constant shift used for all other states. [c] The values less than 0.05 were not listed. For quartet states calculated S_j^2 values were multiplied by a factor of 4/3 due to symmetry reason. [d] The absolute values for the CI coefficients were taken. All molecular orbitals of higher energy than $2a_1'$ were denoted as na_1' or $n'a_1'$.

test whether there might be transitions originating from the $^3A_2'$ state of Al_3O^- to different states of Al_3O, we have calculated the vertical binding energies and pole strength values for those transitions also. In Table 3 we have presented the results using the $^3A_2'$ state geometry (D_{3h} symmetry) of Al_3O^- in the calculation of the Dyson orbital. Similar to the calculations using $^1A_1$ geometry, we have calculated 20 roots for each symmetry states of neutral Al_3O and the ground state for Al_3O^-. Since energetically the $^3A_2'$ state has been found to be slightly higher than the $^1A_1$ state, we have assumed that the lowest energy peak with very small intensity in the observed photoelectron spectrum of Al_3O^- is probably a hot band due to the transition from the $^3A_2'$ state of Al_3O^- to the ground state of Al_3O. On the basis of this, we have adjusted the lowest energy transition from this calculation using the $^3A_2'$ geometry to match the low intensity 1.22 eV vertical ionization peak of the spectrum. All other binding energies have been shifted by the same constant. In this table, the states having pole strength values 0.05 or larger have been reported. From this table it can be seen that the low-energy primary hole states are mainly due to the ionization from $3e'$, $2e'$, $2a_1'$, and $1a_2''$ orbitals. All other states are $2h-1p$ states.

The next level of calculation was MRSDCI calculations for the lowest few roots of the CI matrix of each symmetry to cover the range up to binding energies of approximately 8 eV. For each symmetry, the dominant configurations from the $2h-1p$ CI calculations (coefficient greater than 0.05) were used as the reference space and perturbation theory was used to select approximately 120 000 to 170 000 configurations for each symmetry. MRSDCI calculations were done for both $^1A_1$ and $^3A_2'$ geometries. Similarly for the negative ion of Al_3O, MRSDCI calculations provided the ground-state wave function for computing the Dyson orbitals and the corresponding pole strength. The calculated negative ion ground states energies were

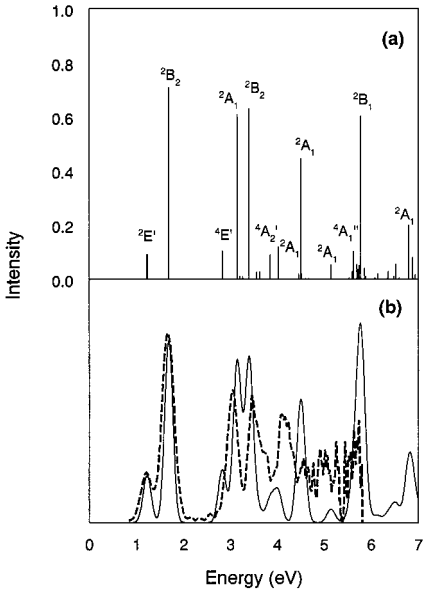

Figure 3. (a) Theoretical spectrum obtained using the calculated energies and pole strength values from $2h-1p$ calculations. The energies have been shifted and scaled to make the first two peaks agree with experiment. (b) Comparison between the experimentally observed and theoretically derived photoelectron spectrum of Al_3O^-. The dashed line represents the experimental spectrum and solid line represents the theoretically simulated spectrum.

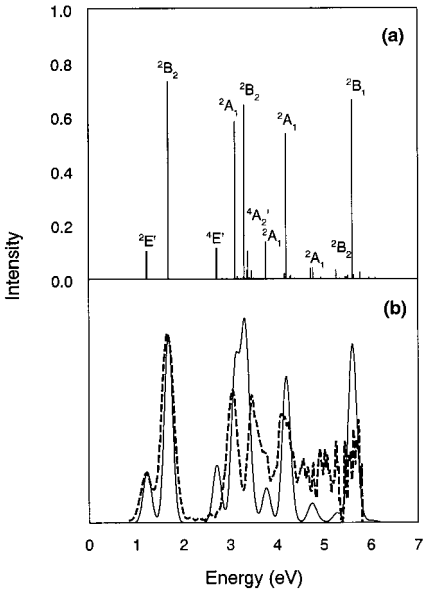

Figure 4. (a) Theoretical spectrum obtained using the calculated energies and pole strength values from MRSDCI calculations. The peaks have been shifted and scaled to make the first two peaks agree with experiment (b) Comparison between the experimentally observed and theoretically derived photoelectron spectrum of Al_3O^-. The dashed line represents the experimental spectrum and solid line represents the theoretically simulated spectrum.

$-801.054\ 371$ and $-801.053\ 557$ au for the $^1A_1$ and $^3A_2'$ states, respectively.

Our best interpretation of the binding energy spectrum of Al_3O^- using the $2h-1p$ and MRSDCI results obtained in the present work have been reported in Figures 3 and 4, respectively. In these plots, the energy differences from the lowest peak have been scaled to agree with the next peaks and the remaining energy differences have been scaled by the same factor. Qualitatively, both of the calculated spectra are similar. The peak positions and intensities corresponding to the line spectrum

of Figures 3a and 4a have been utilized to generate a pseudo-spectrum, based on equal width Gaussians with heights proportional to the calculated weights, and are plotted as Figures 3b and 4b, respectively. For the purpose of comparison, the experimental spectra[18] are plotted in Figures 3b and 4b as dashed lines. It is interesting to note that after exact matching of the first two calculated peaks with the experiment, the calculated peak positions and intensities for the rest of the spectrum are found to agree very well with the experimental spectrum considering that no transition moment factors and no vibrational effects have been included.

In the calculated spectrum, the very low intensity features shown in the stick spectrum of Figures 3a and 4a are not visible in the smoothed spectrum in Figures 2b and 3b due to the Gaussian widths of the more intense peaks. On the basis of the present theoretical results, it is evident that there are two different geometries ($^1A_1$ and $^3A_2'$ state) of the negative ion of Al_3O involved in the photoelectron spectrum. The very first low intensity peak was not assigned to any electronic state by Wu et al. In our results, it is assigned as $(3e')^{-1}\ ^2E' \leftarrow {}^3A_2'$. There is no ambiguity regarding the second peak which has been correctly assigned by Wu et al. as $(3b_2)^{-1}\ ^2B_2 \leftarrow {}^1A_1$. The third peak, which was assigned by Wu et al. as $A\ ^2B_1 \leftarrow {}^1A_1$ on the basis of the typing error in the Boldyrev and Schleyer paper,[13] has been found to be $(4a_1)^{-1}\ ^2A_1 \leftarrow {}^1A_1$. Some low-energy satellite structure between the second and third peak (not assigned by Wu et al.) is due to the $(2e')^{-1}\ ^4E' \leftarrow {}^3A_2'$ transition. The fourth peak, which was previously assigned as $^2A_1$, has been found to be $(2b_2)^{-1}\ ^2B_2 \leftarrow {}^1A_1$ in our assignment. After the fourth peak position, there are some shoulders which we find to be due to the $(2a_1')^{-1}\ ^4A_2' \leftarrow {}^3A_2'$ and $(3b_2)^{-2}(5a_1)^1\ ^2A_1 \leftarrow {}^1A_1$ transitions. The fifth peak has been assigned as $(3a_1)^{-1}\ ^2A_1 \leftarrow {}^1A_1$ by both us and Wu et al. The photoelectron peaks around 5 eV energy were not well resolved experimentally and were not assigned to any transition. We predict that these are due to low-intensity satellites originating from $^1A_1$ as well as a $(1a_2')^{-1}\ ^4A_1'' \leftarrow {}^3A_2'$ primary hole transition. At around 5.8 eV energy, we expect intensity due to the $(1b_1)^{-1}\ ^2B_1 \leftarrow {}^1A_1$ transition.

Summary

The equilibrium geometries of the low lying electronic states of Al_3O and Al_3O^- have been calculated using CASSCF, UB3LYP, and CCD levels of theory. Within the C_{2v} symmetry, the calculated global minimum for Al_3O and Al_3O^- were found to be $^2B_2$ and $^1A_1$ with respective highest occupied molecular orbital occupations $(3b_2)^1$ and $(3b_2)^2$. The $^3A_2'$ state of Al_3O^- was found to have D_{3h} symmetry and slightly higher energy than the corresponding C_{2v} symmetry $^1A_1$ state. It has been found that the $^1A_1$ configuration $(5a_1)^2$, the $^1B_2$ configuration $(3b_2)^1$-$(5a_1)^1$ and $^2A_1$ with a $(5a_1)^1$ configuration are all transition states on the respective potential energy surfaces for pseudorotation. Using the calculated geometries of Al_3O^- at CCD level of theory, configuration interaction (CI) calculations have been done to determine the low-lying vertical excited states of Al_3O, and those results have been utilized to interpret the recently reported experimental photoelectron spectrum of Al_3O^-. Some of the previous assignments for the photoelectron peaks in the observed spectrum were found to be incorrect and new assignments have been made for those peaks.

Acknowledgment. This work was supported by grant number CHE-9613944 from the National Science Foundation.

References and Notes

(1) See, for example: Desjardins, S. J.; Bawagan, A. D. O.; Liu, Z. F.; Tan, K. H.; Yang, Y.; Davidson, E. R. *J. Chem. Phys.* **1995**, *102*, 6385, and references therein.

(2) Bawagan, A. D. O.; Desjardins, S. J.; Dailey, R.; Davidson, E. R. *J. Chem. Phys.* **1997**, *107*, 4295.

(3) Moghaddam, M. S.; Desjardins, S. J.; Bawagan, A. D. O.; Tan, K. H.; Yang, Y.; Davidson, E. R. *J. Chem. Phys.* **1995**, *103*, 10537.

(4) Rolke, J.; Zheng, Y.; Brion, C. E.; Yang, Y. A.; Davidson, E. R. *Chem. Phys.* **1998**, *230*, 153.

(5) Bawagan, A. D. O.; Ghanty, T. K.; Davidson, E. R.; Tan, K. H. *Chem. Phys. Lett.* **1998**, *287*, 61.

(6) Ghanty, T. K.; Davidson, E. R. *Mol. Phys.*, in press.

(7) Cederbaum, L. S.; Domcke, W.; Schirmer, J.; von Niessen, W. *Adv. Chem. Phys.* **1986**, *65*, 115.

(8) *Metal Clusters*; Moskovits, M., Ed.; Wiley: New York, 1986.

(9) *Physics and Chemistry of Small Clusters*; Jena, P., Rao, B. K., Kanna, S. N., Eds.; NATO Advanced Science Institutes Series 158; Plenum: New York, 1987.

(10) Cox, D. M.; Trevor, D. J.; Whitten, R. L.; Rohling, E. A.; Kaldor, A. J. *J. Chem. Phys.* **1986**, *84*, 4651.

(11) Kudo, H. *Nature* **1992**, *355*, 432.

(12) Wang, S. L.; Ledingham, K. W. D.; Singhal, R. P. *J. Phys. Chem.* **1996**, *100*, 11282.

(13) Boldyrev, A. I.; Schleyer, P. v. R. *J. Am. Chem. Soc.* **1991**, *113*, 9045.

(14) Boldyrev, A. I.; Shamovsky, I. L.; Schleyer, P. v. R. *J. Am. Chem. Soc.* **1992**, *114*, 6469.

(15) Vyacheslav, V. G.; Niessen, W. v.; Boldyrev, A. I.; Schleyer, P. v. R. *Chem. Phys.* **1993**, *174*, 167.

(16) Boldyrev, A. I.; Simons, J.; Zakrzewski, V. G.; Niessen, W. v. *J. Phys. Chem.* **1994**, *98*, 1427.

(17) Schleyer, P. v. R.; Kapp, J. *Chem. Phys. Lett.* **1996**, *255*, 363.

(18) Wu, H.; Li, X.; Wang, X. B.; Ding, C. F.; Wang, L. S. *J. Chem. Phys.* **1998**, *109*, 449.

(19) *Gaussian 94*; Frisch, M. J.; Trucks, G. W.; Schlegel, H. B.; Gill, P. M. W.; Johnson, B. G.; Robb, M. A.; Cheeseman, J. R.; Keith, T. A.; Peterson, G. A.; Montgomery, J. A.; Raghavachari, K.; Al-Laham, M. A.; Zakrzewski, V. G.; Ortiz, J. V.; Foresman, J. B.; Cioslowski, J.; Stefanov, B. B.; Nanayakkara, A.; Challacombe, M.; Peng, C. Y.; Ayala, P. Y.; Chen, W.; Wong, M. W.; Andres, J. L.; Replogle, E. S.; Gomperts, R.; Martin, R. L.; Fox, D. J.; Binkley, J. S.; Defrees, D. J.; Baker, J.; Stewart, J. P.; Head-Gordon, M.; Gonzalez, C.; Pople, J. A. Gaussian, Inc., Pittsburgh, PA, 1995.

(20) Dupuis, M.; Marquez, A.; Davidson, E. R. "HONDO 95.6", IBM Corp., Neighborhood Road, Kingston, NY 12401, 1995.

(21) MELD is a set of electronic structure programs written by McMurchie, L. E.; Elbert, S. T.; Langhoff, S. R.; Davidson, E. R., with extensive modifications by Feller, D.; Rawlings, D. C.

(22) Dunning, T. H., Jr. *J. Chem. Phys.* **1989**, *90*, 1007. Woon, D. E.; Dunning, T. H., Jr. *J. Chem. Phys.* **1993**, *98*, 1358. Kendall, R. A.; Dunning, T. H., Jr.; Harrison, R. J. *J. Chem. Phys.* **1992**, *96*, 6769. Basis sets were obtained from the Extensible Computational Chemistry Environment Basis Set Database, Version 1.0, as developed and distributed by the Molecular Science Computing Facility, Environmental and Molecular Sciences Laboratory, which is part of the Pacific Northwest Laboratory, P.O. Box 999, Richland, WA 99352, and funded by the U.S. Department of Energy. The Pacific Northwest Laboratory is a multiprogram laboratory operated by Battelle Memorial Institute for the U.S. Department of Energy under contract DE-AC06-76RLO 1830. Contact David Feller, Karen Schuchardt, or Don Jones for further information.

(23) Feller, D.; Davidson, E. R. *J. Chem. Phys.* **1981**, *84*, 3977.

(24) Davidson, E. R. *J. Am. Chem. Soc.* **1977**, *99* 397.

(25) Pearson, R. G. *J. Am. Chem. Soc.* **1969**, *91*, 4947. Borden, W. T.; Davidson, E. R.; Hart, P. *J. Am. Chem. Soc.* **1978**, *100*, 388.